A LETTERS JOURNAL EXPLORING THE FRONTIERS OF PHYSICS

edp sciences IOP Institute of Physics

LETTER

Design of ultrathin thermal meta-substrate for uniform cooling

To cite this article: Ju Liu *et al* 2021 *EPL* **135** 26003

View the article online for updates and enhancements.

This content was downloaded from IP address 210.42.111.81 on 03/10/2021 at 05:56

A LETTERS JOURNAL EXPLORING THE FRONTIERS OF PHYSICS

July 2021

EPL, **135** (2021) 26003
doi: 10.1209/0295-5075/ac0ad6

www.epljournal.org

Design of ultrathin thermal meta-substrate for uniform cooling

JU LIU[1], XUECHENG REN[2] and RUN HU[2(a)]

[1] *Guangdong Polytechnic - Foshan 528041, Guangdong, China*
[2] *School of Energy and Power Engineering, Huazhong University of Science and Technology Wuhan 430074, China*

received 26 March 2021; accepted in final form 11 June 2021
published online 29 September 2021

Abstract – Thermal metamaterials have been demonstrated to be powerful on heat manipulation and promising for thermal management in recent years, but most thermal functionalities remain in theory, and thus practical applications of thermal metamaterials are extremely urgent and worth exploring. Here, by drawing inspiration from the uniform top temperature distribution of vapor chamber that enables efficient electronics cooling, we design a thermal meta-substrate for achieving uniform top temperature profile under the design framework of the illusion thermotics theory. Further, the key parameter for better uniform cooling is identified as the length of illusion heat source by parameter optimization. Such an all-solid substrate not only combines the advantages of metamaterials and the uniform top temperature distribution of vapor chamber, but also breaks the thickness limit of the conventional liquid-based vapor chamber toward ultrathin thickness. It is expected that the present substrate concept can be used for electronics cooling and trigger further exploration on the practical application of thermal metamaterials.

Copyright © 2021 EPLA

Introduction. – Thermal metamaterials, as a great branch of artificially structured metamaterials, have garnered increasing attention in recent decades as they exhibit extraordinary thermal properties beyond conventional naturally occurring materials that enable the flexible manipulation of heat almost at will. Based on thermal metamaterials, many novel thermal metadevices have been proposed and demonstrated theoretically and experimentally, such as thermal cloaking [1–7], concentrating [2,8–10], rotating [2,11], camouflage [12–19], encoding [20] and encrypted printing [21], etc. Heat conduction is usually omnidirectional in conventional thermal materials, while in thermal metamaterials the directional heat conduction is enabled, thus rendering great potential for the thermal management of electronics. However, most thermal functionalities based on thermal metamaterials remain in theory or lack of practical applications. A remarkable example is the thermal-metamaterials–based printed circuit board by integrating the thermal cloaking, concentrating, and rotating units on one substrate to modulate heat flow from the chips to the external heat sink [22,23]. It is thus extremely urgent to further explore the practical applications of thermal metamaterials.

Thermal management has been considered as the key bottleneck for the further development of high-power electronics toward extreme miniaturization, multifunctionalities, and application scenarios [24,25]. To achieve efficient thermal management, high thermal conductivity materials for chips, packages, and device and structure optimizations have been extensively and intensively explored. As for the packaging level, two main challenges remain to be solved. One is the low thermal conductivity of the multilayer composite substrate leading to the large bulk thermal resistance, and the other is the large size change between the chips and the substrates resulting in large spreading thermal resistance. To solve this, researchers have proposed the concept and device of heat pipe or vapor chamber [26–28]. In vapor chambers, as shown in fig. 1(a), heat is absorbed by the small-size heat sources (chips) at the bottom, and the working vapor condenses at the whole top surface with uniform temperature to enhance the heat dissipation efficiency of the external heat sink. Via vapor chambers, both the spreading thermal resistance and the bulk thermal resistance are overcome efficiently due to the uniform top temperature, thus vapor chambers have been extensively used in high-performance computers, laptops, and cellphones. Nevertheless, the vapor chamber has been developed toward ultrathin thickness, but the challenges like system complexity, sufficient capillary force, evaporation limit, vapor diffusion limit, and capillary flow limits, should be tackled [26–28].

(a)E-mail: hurun@hust.edu.cn (corresponding author)

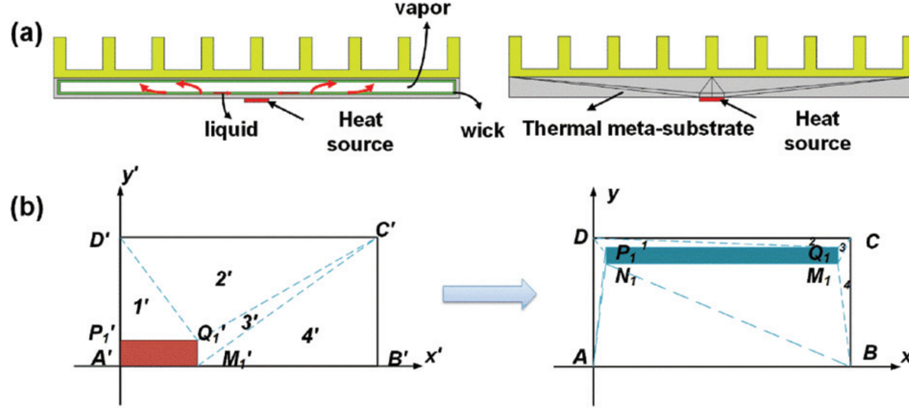

Fig. 1: (a) Schematic of vapor chamber and the thermal meta-substrate. (b) Schematic of the illusion thermotics design process.

Noting the advantages of uniform top temperature distribution in vapor chambers and thermal metamaterials, here comes one idea naturally, that is can we combine these two together to achieve the uniform top temperature to enable efficient uniform cooling? To examine the feasibility, in this study, we further extend the regionalization transformation method to design a thermal meta-substrate with uniform top temperature distribution for efficient cooling. It is worth noting that the proposed meta-substrate is all solid, avoiding the limits of conventional liquid-based vapor chambers, and thus it is promising toward ultrathin thickness. Detailed design processes were introduced and finite-element simulations were conducted for validation and optimization.

Methodology. – As shown in fig. 1(a), we replaced the same space of the vapor chamber by the proposed all-solid meta-substrate, and the cooling performance was estimated by the top temperature via FEM simulations. The thermal meta-substrate was designed by the regionalization transformation method that was proposed in our previous papers [12,19,21]. Following a similar method, both the two- and three-dimensional substrates can be designed and for simplicity we introduced the 2D version for better understanding. To start, as shown in fig. 1(b), the real space is denoted by $A'B'C'D'$ and the real heat source is denoted by the $P'Q'M'N'$ respectively, the corresponding illusion space is denoted by $ABCD$ and the illusion heat source is denoted by the $PQMN$, respectively. The dimensions of the real space and the illusion space are both $L \times W$ mm, the real heat source is $l \times w$, and the illusion heat source is $l' \times w'$, respectively. Both the illusion and real spaces are divided into some triangular subspaces. The real space is divided into four triangles denoted by numbers from $1'$ to $4'$, and the corresponding triangle regions in the virtual space are denoted by numbers from 1 to 4. According to the coordinate transformation relationship [12], each point (x, y, z) in each triangle region can then be mapped to the new one (x', y', z') in the corresponding triangle by the following linear relationship:

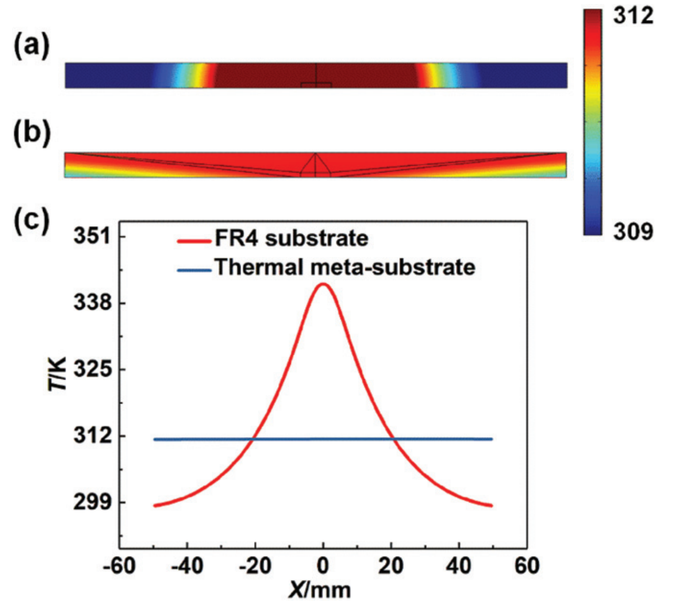

Fig. 2: Comparison of temperature fields for (a) homogenous FR4 substrate, (b) thermal meta-substrate, and (c) top temperature profiles of the two substrates.

$$\begin{bmatrix} x_i' \\ y_i' \\ z_i' \end{bmatrix} = \begin{bmatrix} \alpha_i & \beta_i & \gamma_i & \varphi_i \\ \mu_i & \nu_i & \varepsilon_i & \theta_i \\ \lambda_i & \sigma_i & \rho_i & \omega_i \end{bmatrix} \begin{bmatrix} x_i \\ y_i \\ z_i \\ 1 \end{bmatrix}, \tag{1}$$

where α, β, γ, φ, μ, ν, ε, θ and ω are the nine undetermined coefficients, subscript index i denotes the i-th triangle section, and the superscript denotes the transformed space.

The anisotropic thermal conductivity κ_i' in each subspace can be calculated from the transformation thermotics as

$$\kappa_i' = \begin{bmatrix} \kappa_{xx}' & \kappa_{xy}' & \kappa_{xz}' \\ \kappa_{yx}' & \kappa_{yy}' & \kappa_{yz}' \\ \kappa_{zx}' & \kappa_{zy}' & \kappa_{zz}' \end{bmatrix} = \frac{\mathbf{J}_i \kappa_0 \mathbf{J}_i^{\mathrm{T}}}{\det(\mathbf{J}_i)}, \tag{2}$$

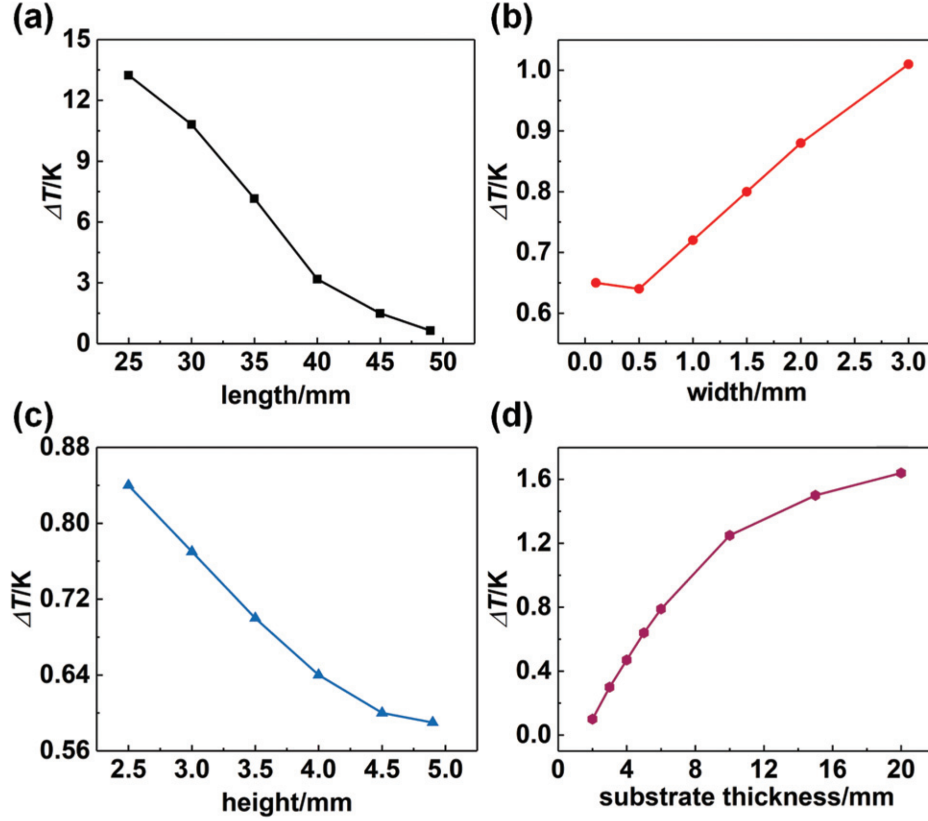

Fig. 3: Influence of size parameters on the thermal meta-substrate performance. (a) Illusion source length l', (b) illusion source width w', (c) illusion source height (the position of point P), and (d) substrate thickness W.

where κ_0 is the homogeneous thermal conductivity in the illusion space and $\mathbf{J}_i$ is the Jacobian matrix of the coordinate transformation as

$$\mathbf{J}_i = \frac{\partial(x_i', y_i', z_i')}{\partial(x_i, y_i, z_i)} = \begin{bmatrix} \alpha_i & \beta_i & \gamma_i \\ \mu_i & \nu_i & \varepsilon_i \\ \lambda_i & \sigma_i & \rho_i \end{bmatrix}.$$

$\mathbf{J}_i^{\mathrm{T}}$ is the transpose matrix of $\mathbf{J}_i$. Note that for the 2D version, the procedure is the same and the only difference is the number of the subspace (triangles). To achieve the uniform top temperature profile, we designed the illusion heat source with a long rectangle shape located close to the top surface, as shown in the left image of fig. 1(b).

Results and discussion. – By using COMSOL (`https://www.comsol.com`), we perform finite-element simulations to confirm the validity of ultrathin thermal meta-substrate for uniform cooling. In the first validation, the thermal meta-substrate is symmetric to the y-axes. The dimensions of the half-substrate in the first quadrant are $50 \times 5\,\mathrm{mm}^2$. And the real heat source of the half-substrate in the first quadrant is located at the origin with dimension of $3 \times 1\,\mathrm{mm}^2$, and that of the illusion targets are $49 \times 1\,\mathrm{mm}^2$. The illusion heat source is located at P (0.5, 4) mm with dimensions of $PQ = 49\,\mathrm{mm}$ and $PN = 1\,\mathrm{mm}$ without rotation. The volumetric power of the heat source (real heat source $P'Q'M'N'$) is 10 watts. The boundary lines $A'B'$ and $A'D'$ are kept adiabatic while the other two are cooled by natural convection with a convection coefficient of $5\,\mathrm{W/(m^2 \cdot K)}$ at room temperature. The simulation results are shown in fig. 2. As a comparison, the simulated temperature field of the homogeneous FR4 substrate is shown in fig. 2(a), in which the real heat source is located at the center on the bottom line. The thermal conductivity of the homogeneous FR4 substrate is $0.3\,\mathrm{W/(m \cdot K)}$. It is seen in fig. 2(a) and (b) that the temperature distribution is uniform on the top of the thermal meta-substrate obviously while the temperature field of the FR4 substrate is rather non-uniform. We extract the temperatures of the top surface of the two substrates and plot them in fig. 2(c). It is seen that the temperature on the top surface of the thermal meta-substrate is almost equal, while the temperature distribution is not uniform for the FR4 substrate. The temperature difference ΔT between the maximum and the minimum temperature on the top surface is 0.09 K and 43.41 K for the thermal meta-substrate and the FR4 substrate, respectively. Rather good temperature uniformity on the thermal metamaterial substrate is achieved, just like an equivalent vapor chamber's thermal performance.

To further test the influence of size parameters, including length, width and height of illusion heat source (y-coordinate of point P) and substrate thickness on the thermal performance, we perform the finite-element method (FEM) simulations with the calculated thermal

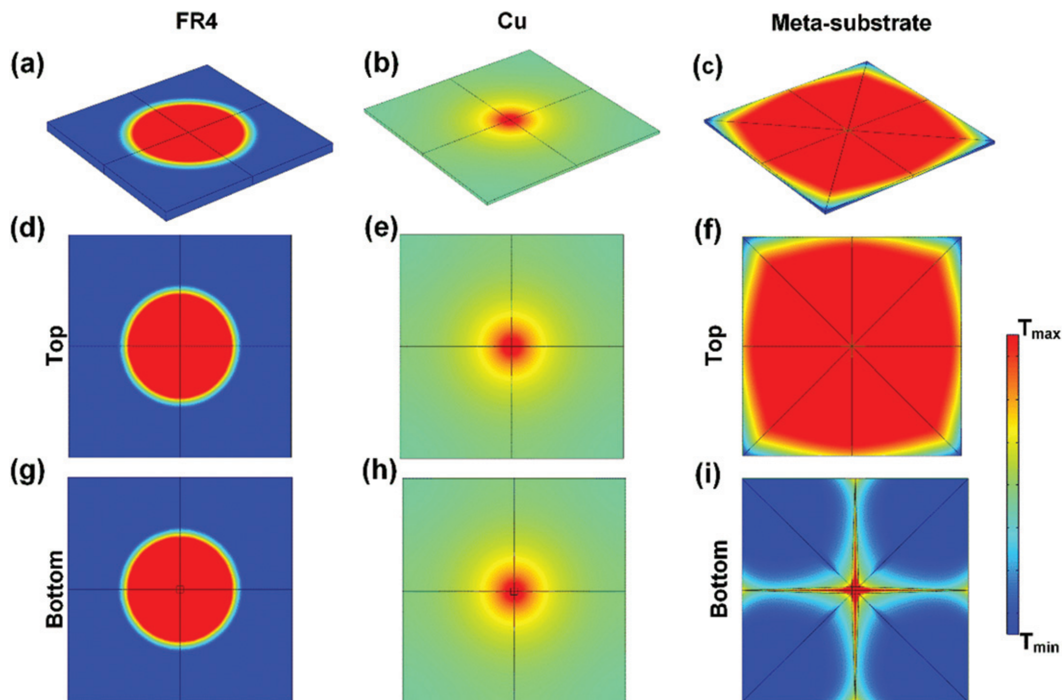

Fig. 4: FEM temperature field comparisons between the homogenous FR4 substrate (the left column), Cu substrate (the middle column) and the thermal meta-substrate (the right column): (a)–(c) 3D temperature field; (d)–(f) top surface; and (g)–(i) bottom surface.

conductivity tensors. In the FEM simulation, the heat source is located at the original point with 10 watt power. The anisotropic thermal conductivities of the 4 triangular subspaces are calculated according to eq. (2) independently. The simulation results are shown in fig. 3. It is seen in fig. 3(a) that with the increase of length l', ΔT decreases monotonously. With the increase of length from 25, 30, 35, 40, 45, to 49 mm, the temperature difference ΔT becomes smaller from 10.81 K, 13.24 K, 7.15 K, 3.18 K, 1.49 K, to 0.64 K, implying a more uniform top temperature performance. It is seen in fig. 3(b) that with the increase of width w' from 0.1, 0.5, 1, 1.5, 2, to 3 mm, the temperature difference ΔT becomes larger from 0.65 K, 0.64 K, 0.72 K, 0.8 K, 0.88 K, to 1.01 K. It is seen in fig. 3(c) that with the increase of height h' of the illusion heat source, corresponding to the position of point P, from 2.5, 3.0, 3.5, 4.0, 4.5, to 4.9 mm, the temperature difference ΔT becomes smaller from 0.84 K, 0.77 K, 0.7 K, 0.64 K, 0.6 K, to 0.59 K, implying a more uniform top temperature performance. It is seen in fig. 3(d) that with the increase of the substrate thickness from 2, 3, 4, 5, 6, 10, 15, to 20 mm, the temperature difference ΔT becomes larger from 0.1 K, 0.3 K, 0.47 K, 0.64 K, 0.79 K, 1.25 K, 1.5 K, to 1.64 K, implying worse performance of uniform temperature distribution at the top surface. To summarize, it is seen that a good performance of the uniform top temperature profile corresponds to longer length, larger height, smaller width, and smaller substrate thickness. The meta-substrate is all solid, thus can break the limits of the conventional liquid-based vapor chamber. As long as the desired thermal conductivity can be achieved, the meta-substrate can be designed and fabricate toward ultrathin thickness. Moreover, the illusion heat source length is the key parameter among these variables, corresponding to a more significant influence on the temperature uniformity (larger temperature difference ΔT).

We also perform FEM simulations to validate the three-dimensional ultrathin thermal meta-substrate for uniform cooling. In our design, the dimensions of the quarter substrate in the first quadrant are length $L = 100$ mm, width of $W = 100$ mm and height of $H = 3$ mm. The real heat source of the quarter substrate is located at the center on the bottom of the substrate with dimensions $l' = 3$ mm, $w' = 3$ mm, and $h' = 1$ mm. The dimensions of the illusion heat source are $l = 85$ mm, $w = 85$ mm and $h = 0.3$ mm. In our model, the cuboid substrate can be divided into 18 tetrahedron regions. The coordinates of the thermal illusion are positioned by point P at (10, 10, 0). The anisotropic thermal conductivities of the 18 tetrahedron regions are calculated according to eq. (2). In the FEM simulation, the volumetric power of the heat source is 50 watts. All the boundaries are cooled by natural convection with convection coefficient of $5\,\mathrm{W/(m^2 \cdot K)}$ and ambient air temperature at $20\,^{\circ}\mathrm{C}$. The simulation results are shown in fig. 4(c). As a comparison, the simulated temperature field of a homogenous FR4 substrate is shown in fig. 4(a). In addition, we perform the simulation of a Cu substrate as shown in fig. 4(b). Due to the isotropic heat conduction of Cu or FR4, both the hot spot (maximum temperature point) on the top and bottom planes

are located at the center as shown in figs. 4(d), (g) and (e), (h). The top surface temperature profile of thermal meta-substrate as shown in fig. 4(f) indicates that the thermal meta-substrate achieves the effect of equivalent vapor chamber. As shown in fig. 4(i), it is seen that although the real heat source is located in the center bottom of the substrate, the uniform temperature distribution is observed from the top surface of the substrate instead. The comparison of temperature profiles of the top surfaces on the three substrates in fig. 4 obviously indicates that the present meta-substrate can work with a uniform temperature profile on the top surface for efficient uniform cooling, and the non-uniform bottom temperature is due to the non-uniform heat source and will not matter but benefit for practical application.

Conclusion. – In summary, we apply the illusion thermotics theory to design a meta-substrate, which works with a uniform temperature profile on the top surface for efficient uniform cooling. Such an all-solid substrate not only combines the advantages of metamaterials and vapor chamber, but also breaks the thickness limits of the conventional liquid-based vapor chamber. The detailed design processes were presented, and the working performance was verified by finite-element simulations. FEM simulations validate that although the real heat source is located at the bottom center, uniform temperature distributions are observed on the top surface of the substrate. Parameter optimization was conducted to identify the key parameter as the length of the illusion heat source. Although the anisotropic thermal conductivities cannot be found directly from the nature world, we may fabricate it via layered materials [2], composite materials [12], or 3D printing [29] and so on. We will further explore the feasible fabrication of the meta-substrate and the related practical applications. The present thermal-metamaterials–based substrate concept can be used for electronics cooling and trigger more the practical application of thermal metamaterials.

* * *

The authors acknowledge the financial support from the Wuhan City Science and Technology Program (2020010601012197), National Natural Science Foundation of China (52076087, 51706079), and Young Innovative Talent Program of Guangdong Province (2018GkQNCX025).

Data availability statement: The data that support the findings of this study are available upon reasonable request from the authors.

REFERENCES

[1] Fan C. Z., Gao Y. and Huang J. P., *Appl. Phys. Lett.*, **92** (2008) 251907.

[2] Narayana S. and Sato Y., *Phys. Rev. Lett.*, **108** (2012) 214303.

[3] Han T. C., Bai X., Gao D. L., Thong J. T. L., Li B. W. and Qiu C. W., *Phys. Rev. Lett.*, **112** (2014) 054302.

[4] Li Y., Shen X. Y., Wu Z. H., Huang J. Y., Chen Y. X., Ni Y. S. and Huang J. P., *Phys. Rev. Lett.*, **115** (2015) 195503.

[5] Zhu Z., Ren X., Sha W., Xiao M., Hu R. and Luo X., *Int. J. Heat Mass Transfer*, **176** (2021) 121417.

[6] Schittny R., Kadic M., Guenneau S. and Wegener M., *Phys. Rev. Lett.*, **110** (2013) 195901.

[7] Lan C., Li B. and Zhou J., *Opt. Exp.*, **23** (2015) 3478.

[8] Hu R., Wei X., Hu J. and Luo X., *Sci. Rep.*, **4** (2014) 3600.

[9] Guenneau S., Amra C. and Veynante D., *Opt. Exp.*, **20** (2012) 8207.

[10] Guenneau S. and Amra C., *Opt. Exp.*, **21** (2013) 6578.

[11] Zhou L., Huang S., Wang M., Hu R. and Luo X., *Phys. Lett. A*, **383** (2019) 759.

[12] Hu R., Zhou S. L., Li Y., Lei D. Y., Luo X. B. and Qiu C. W., *Adv. Mater.*, **30** (2018) 1707237.

[13] Li J. X., Li Y., Cao P. C., Yang T. Z., Zhu X. F., Wang W. Y. and Qiu C. W., *Adv. Mater.*, **32** (2020) 2003823.

[14] Zhou S. L., Hu R. and Luo X. B., *Int. J. Heat Mass Transfer*, **127** (2018) 607.

[15] Li Y., Zhu K. J., Peng Y. G., Li W., Yang T. Z., Xu H. X., Chen H., Zhu X. F., Fan S. H. and Qiu C. W., *Nat. Commun.*, **18** (2019) 48.

[16] Han T. C., Bai X., Thong J. T. L., Li B. W. and Qiu C. W., *Adv. Mater.*, **26** (2014) 1731.

[17] Li Y., Bai X., Yang T., Luo H. and Qiu C. W., *Nat. Commun.*, **9** (2018) 273.

[18] Peng Y. G., Li Y., Cao P. C. and Zhu X. F., *Adv. Funct. Mater.*, **30** (2020) 2002061.

[19] Peng X. Y. and Hu R., *ES Energy Environ.*, **6** (2019) 39.

[20] Hu R., Huang S. Y., Wang M., Zhou L. L., Peng X. Y. and Luo X. B., *Phys. Rev. Appl.*, **10** (2018) 054032.

[21] Hu R., Huang S. Y., Wang M., Luo X. B., Shiomi J. and Qiu C. W., *Adv. Mater.*, **31** (2019) 1807849.

[22] Dede E. M., Nomura T., Schmalenberg P. and Lee J. S., *Appl. Phys. Lett.*, **103** (2013) 063501.

[23] Dede E. M., Zhou F., Schmalenberg P. and Nomura T., *J. Electron. Packag.*, **140** (2018) 010904.

[24] Lan W., Shang B. F., Wu R. K., Yu X. J. and Luo X. B., *Int. J. Therm. Sci.*, **159** (2020) 106619.

[25] Shang B., Wu R., Hu J., Hu R. and Luo X., *Int. J. Therm. Sci.*, **131** (2018) 20.

[26] Solomona Brusly A., Sekara M. and Yang S. H., *Appl. Therm. Eng.*, **100** (2016) 462.

[27] Ghanbarpoura A., Hosseinib M. J., Ranjbara A. A., Rahimib M., Bahrampouryc R. and Ghanbarpour M., *Renew. Energy*, **163** (2021) 698.

[28] Chen L., Deng D. X., Huang Q. S., Xu X. H. and Xie Y. X., *Appl. Therm. Eng.*, **166** (2020) 114686.

[29] Peng Y. G., Li Y., Cao P. C., Zhu X. F. and Qiu C. W., *Adv. Funct. Mater.*, **30** (2020) 202002061.